

## 28.1 A Handheld 50pM-Sensitivity Micro-NMR CMOS Platform with B-Field Stabilization for Multi-Type Biological/Chemical Assays

Ka-Meng Lei<sup>1</sup>, Hadi Heidari<sup>2,3</sup>, Pui-In Mak<sup>1</sup>, Man-Kay Law<sup>1</sup>, Franco Maloberti<sup>2</sup>, Rui P. Martins<sup>1,4</sup>

<sup>1</sup>University of Macau, Macau, China,

<sup>2</sup>University of Pavia, Pavia, Italy,

<sup>3</sup>University of Glasgow, Glasgow, United Kingdom,

<sup>4</sup>Instituto Superior Tecnico, Lisbon, Portugal

Point-of-use (PoU) biological/chemical assays are aimed to transform bulky laboratory instruments into easy-to-use lab-on-a-chip platforms, bringing down the cost, size, and sample-use by orders of magnitude [1,2]. Micro-Nuclear Magnetic Resonance (NMR) is a trail-blazing tool for *target* pinpointing, by utilizing functionalized magnetic nanoparticles (MNPs) as the *probe* [3]. Screening by micro-NMR is repeatable, versatile and low-cost as it is label- and washing-free for the samples, and immobilization-free for the electrodes. Herein, a high-sensitivity micro-NMR CMOS platform with magnetic (B)-field stabilization and thermal management is reported (Fig. 28.1.1). This handheld tool unifies multi-type assays (target detection, protein state analysis, and solvent-polymer dynamics), and is suitable for healthcare, food industry, and colloidal applications.

Micro-NMR relaxometry detects the spin-spin relaxation time ( $T_2$ ) by extracting the echoes envelopes from the response of the non-zero spin nuclei (i.e.,  $^1\text{H}$ ). The nuclei, under magnetization with a static magnetic field ( $B_0$ ), absorb orthogonal RF exciting magnetic field ( $B_1$ ) at the Larmor frequency,  $f_L = \gamma B_0$  ( $\gamma$ : gyromagnetic ratio), and precess about the direction of magnetization at  $f_L$  even after the cessation of the excitation. In an existing micro-NMR system [3], frequency deviation of the local oscillator (LO) from  $f_L$  induces improper frequency excitation, paralyzing the operation. Confounded by the thermal instability of the portable magnet ( $B_0=0.46\text{T}$ , T.C.=1200ppm/K), LO tracking is essential to safeguard the system against environmental changes.

Our micro-NMR platform (Fig. 28.1.2) is tailored with  $B_0$ -field stabilization and thermal management to enhance the robustness and simplify the hardware. The dynamic  $B_1$ -field transduction is based on a spiral coil driven by a transmitter (TX)/receiver (RX) together with a matching capacitor  $C_m$ , to excite/obtain the magnetic signal to/from the droplet samples (2.5 $\mu\text{L}$ ) normal to the chip surface. The TX is based on a tapped inverter-chain power amplifier (PA), measured 31.6% power efficiency, to deliver programmable pulse sequences pertaining to the LO. The RX features a multi-stage low-noise amplifier (LNA) for high RX sensitivity (down to 1nV/ $\sqrt{\text{Hz}}$  input-referred-noise), and a dynamic-bandwidth lowpass filter for fast recovery from saturation after excitation pulses. The  $B_0$ -field sensor and calibrator manage the lateral  $B_0$ -field together with a current driver, which injects a calibration current to the magnet (75mT/A) stabilizing the bulk magnetization on the nuclei. The spiral coil also serves as a heater allowing thermal profiling of the samples. The thermal-induced error on the  $B_0$ -field sensor and calibrator, and the hotness of the samples, are monitored by a BJT temperature sensor.

To sense the lateral  $B_0$ -field normal to the chip surface, a *current-mode* 4-folded vertical hall sensor (VHS) arranged in a Wheatstone bridge is employed (Fig. 28.1.3). Each VHS element is composed by an n-well as the substrate and three n-diffusions as contacts [4]. P-diffusions are embedded between the n-diffusions to avert current flowing at the surface, soothing the  $1/f$  noise. To achieve sub-nA sensitivity, the VHS readout circuit (Fig. 28.1.3) is based on a low-noise TIA. Current-spinning and chopper are applied reducing the  $1/f$  noise corner by  $>5,000\times$ . Switches  $S_{7,8}$  control the flows of the current and reset the capacitors  $C_F$ . Small switches (280 $\Omega$  each) can exacerbate the impedance of the TIA, ( $R_{in,TIA}=210\Omega$ ) if there is current passing through the switches connected between the core OTA of the TIA and VHS (i.e.,  $S_{7,8}$ ). To address this,  $S_{7,8}$  are managed to guide the current passing through the negative feedback path, nullifying the impact of resistances of  $S_{7,8}$  on the TIA. Thanks to this switching scheme,  $R_{in,TIA}$  is suppressed by 84%, absorbing  $\sim 21\%$  more current into the TIA than the general approach [5].

Attributed to the prodigious nominal  $B_0$ -field, a typical TIA can be saturated and fail to sense the tiny  $B_0$ -field variation (3.75mT). To solve it, a nominal  $B_0$ -field compensator made by a passive switched-capacitor network (Fig. 28.1.3) nullifies the nominal  $B_0$ -field entering into the TIA.

Before the micro-NMR assay, the VHS reads  $B_0$  and responds to the current driver (Fig. 28.1.4).  $B_0$  may shift away from its nominal value due to the environmental changes (e.g., temperature and sample-to-magnet position). Thus, untracked  $f_L$  can be easily off-center from the LO frequency  $f_{osc}$  (BW=16.7kHz). Here, by modulating the magnet according to an updated  $B_0$  (sensitivity: 4.12V/T),  $f_L$  is reset to  $f_{osc}$ . Also, with signal-averaging performed in the frequency domain to suppress the background noise, the calibration improves the  $B_0$ -field stability by  $13\times$  (from 2 to 0.15mT) at 0.46T ( $f_L=19.6\text{MHz}$ ). Under the synergy of micro-NMR and VHS, the stabilized  $f_L$  inspires the use of a simple crystal oscillator as the LO that measures low phase noise ( $-116\text{dBc/Hz}$  at 1kHz offset) at very low power (79 $\mu\text{W}$ ).

Human Immunoglobulin G (IgG), which protects the body from infections, can be quantified by utilizing Protein A coated water-soluble MNPs (i.e.,  $\text{Fe}_2\text{O}_3$ ) based on their  $T_2$ .  $T_2$  of the sample is shortened commensurate with the amount of IgG upon nanoparticles agglomeration, enabling quantification of IgG down to 5nM (Fig. 28.1.5). The specificity of micro-NMR assay is evinced with the addition of Chicken Immunoglobulin Y (IgY), which does not conjugate with Protein A. The negligible change of  $T_2$  ( $<2\%$ ) validates the selectivity of the assay. The versatility of the platform is manifested with DNA detection apt for life-threatening bacteria screening. With a pair of probe-decorated MNPs, the platform quantifies the synthesized DNA derived from *Enterococcus faecalis*, with a detection limit down to 50pM in 2.5 $\mu\text{L}$  samples (125amol). By varying the MNP concentration, the detection range is impelled to 125nM. The response to single-nucleotide polymorphism is indistinguishable to  $T_2$  baseline ( $<4\%$ ), substantiating that single-base mismatch DNA can be differentiated.

Probing the molecular structure can digest the protein state for food quality inspection. Protein  $\beta$ -lactoglobulin ( $\beta$ -LG) denatures and aggregates irreversibly after heating to  $>60^\circ\text{C}$  [6]. This state transformation can be embodied by measuring  $T_2$  of the samples attributed to the dissimilar interaction between the water molecules and protein at different states and sizes (Fig. 28.1.6). For the colloidal industry, Poly(N-isopropylacrylamide) (PNIPAM) is widely used as advanced sensor and drug delivery carrier [7]. It is a colloidal polymer that exhibits a temperature-induced reversible volume phase transition in water, affects the local environment on solvent confinement and thus  $T_2$  of the solvent. By duty-cycling the heater (coil), PNIPAM undergoes a volume phase transition above  $33^\circ\text{C}$ , resulting in  $T_2$  decrement of the solvent.

Benchmarking with the recent PoU tools (Fig. 28.1.7), this work supports multi-type assays in one unified platform, while achieving high sensitivity and selectivity for DNA, as well as other proteins targeting capability in tiny sample with functionalized MNPs. The platform consumes  $120\times$  less samples, and is  $96\times$  lighter,  $175\times$  smaller, and  $16\times$  cheaper than a commercial product (Bruker mq-20 [8]).

### Acknowledgements:

The authors thank Macao FDCT (SKL fund & 047/2014/A1) for financial support.

### References:

- [1] M. Bakhshiani et al., "A Microfluidic-CMOS Platform with 3D Capacitive Sensor and Fully Integrated Transceiver IC for Palmtop Dielectric Spectroscopy," *ISSCC Dig. Tech. Papers*, pp. 386-387, Feb. 2015.
- [2] P.-H. Kuo et al., "A Smart CMOS Assay SoC for Rapid Blood Screening Test of Risk Prediction," *ISSCC Dig. Tech. Papers*, pp. 390-391, Feb. 2015.
- [3] N. Sun et al., "Palm NMR and One-Chip NMR," *ISSCC Dig. Tech. Papers*, pp. 488-489, Feb. 2010.
- [4] G.-M. Sung et al., "2-D Differential Folded Vertical Hall Device Fabricated on a P-Type Substrate Using CMOS Technology" *IEEE Sensors J.*, vol. 13, pp. 2253-2262, June 2013.
- [5] H. Heidari et al., "A CMOS Current-Mode Magnetic Hall Sensor with Integrated Front-end," *IEEE Trans. Circuits Syst. I*, vol. 62, no. 5, pp. 1270-1278, May 2015.
- [6] L. Indrawati et al., "Low-Field NMR: A Tool for Studying Protein Aggregation," *J. Sci. Food Agric.*, vol. 87, pp. 2207-2216, Sept. 2007.
- [7] B. S.-Martin et al., "Structure and Polymer Dynamics within PNIPAM-Based Microgel Particles," *Adv. Colloid Interface Sci.*, vol. 205, pp. 113-123, Mar. 2014.
- [8] Bruker Minispec Contrast Agent Analyzer, [Online]. Available: <https://www.bruker.com/products/mr/td-nmr/minispec-mq-series/mq-contrast-agent-analyzer/overview.html>

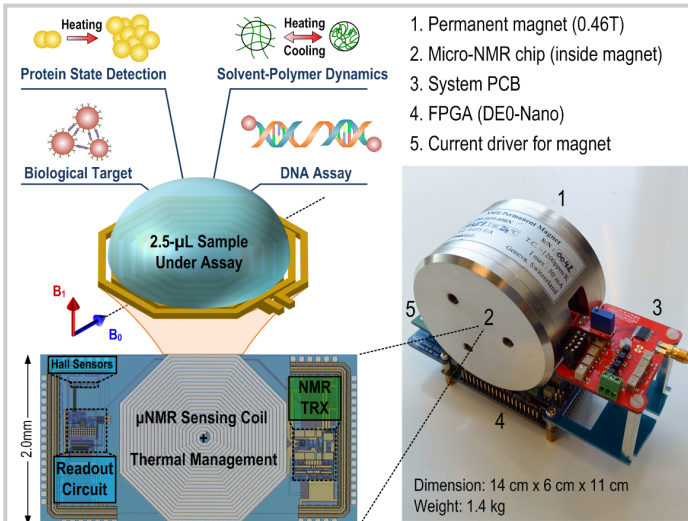


Figure 28.1.1: A micro-NMR CMOS platform with B-field stabilization: (left) chip photo and (right) platform assembly.

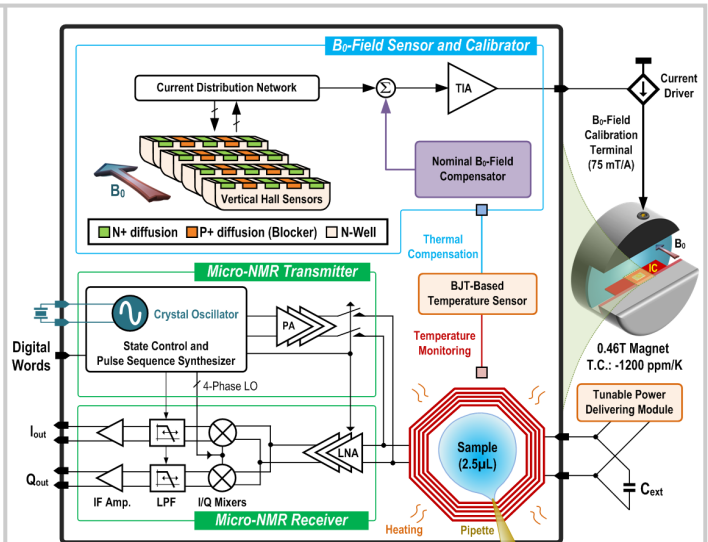


Figure 28.1.2: System block diagram.

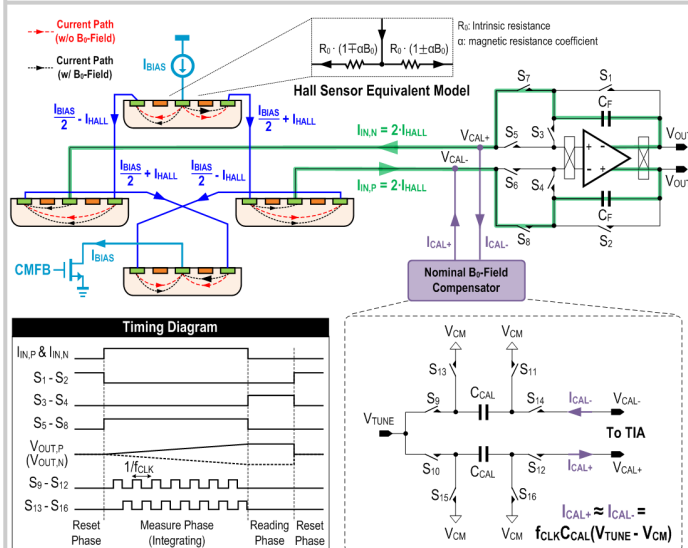


Figure 28.1.3: Current-mode 4-folded VHS to sense the lateral B<sub>0</sub>-field.

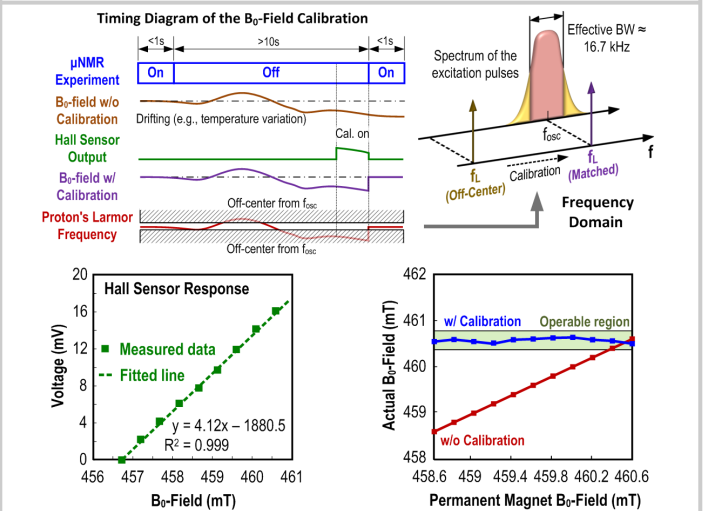


Figure 28.1.4: (Top) Timing diagram of the B<sub>0</sub>-field calibration and its frequency domain illustration. (Bottom) Measured Hall sensor response and B<sub>0</sub>-field with and without calibration.

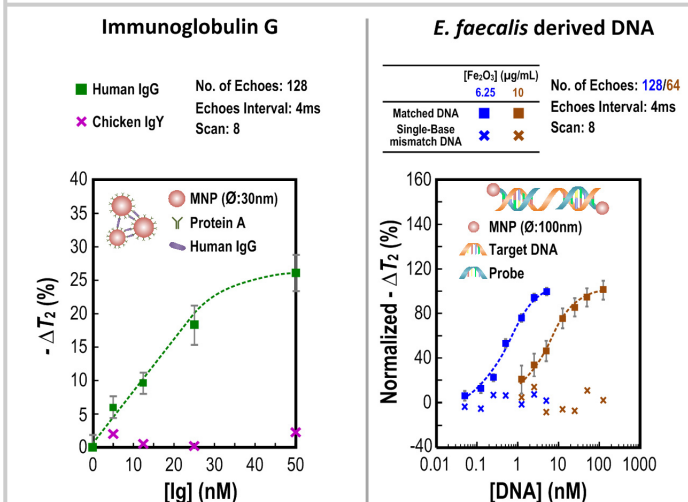


Figure 28.1.5: Examples of target detection: (left) from Human IgG as target, and Chicken IgY as control; (right) from *E. faecalis* derived DNA and single-base mismatch DNA.

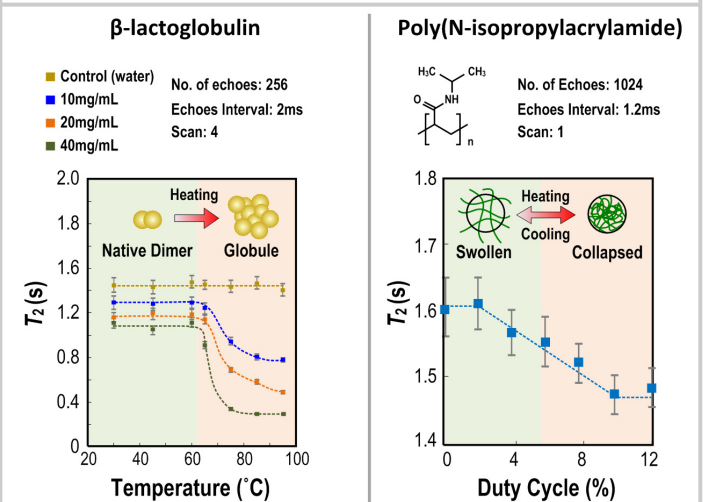


Figure 28.1.6: Examples of state analysis reflected by T<sub>2</sub>: (left) thermal profiling of protein (β-LG) state; (right) polymer (PNIPAM) dynamics during heating and cooling.

		This Work	P.-H. Kuo <i>et al.</i> , ISSCC'15	K.-H. Lee <i>et al.</i> , ISSCC'12	N. Sun <i>et al.</i> , ISSCC'10	B. Jang <i>et al.</i> , ISSCC'09
Application	Specificity	1. Target detection 2. Solvent-Polymer dynamics 3. Protein state analysis	Target detection	Target detection	Target detection	Target detection
	Target Labeling	Label-free	Label-free	Label-free	Label-free	Cy5-label
	Demo Target	68 base <i>E. faecalis</i> derived DNA	NT-ProBNP & TNF-alpha	21 base H5N1 virus	hCG cancer marker	18 base DNA
	Detection Limit	50 pM (DNA)	--	100 pM (DNA)	5000 pM (Cancer marker)	125 pM (DNA)
	Sample Handling Limit	2.5 $\mu$ L	--	--	5.0 $\mu$ L	--
Hardware	Physics	NMR relaxometry + Thermal management	Magnetic- sensing	Capacitance- sensing	NMR relaxometry	Fluorescent- sensing
	Post-Fabrication Necessity	No (immobilization free)	Probe (antibody) immobilization	Probe (DNA) immobilization on Au electrodes	No (immobilization free)	Fiber-optical faceplate
	External Part	Portable magnet	No	No	Portable magnet	Light source
	LO Generation	Crystal oscillator + $B_0$ -field calibration	--	--	Off-chip	--
	Robustness to environments	Robust to temperature & sample position variations	Robust to temperature variation	Vulnerable to bias current variation	Vulnerable to B-field variation	Vulnerable to background noise
	CMOS Tech.	0.18 $\mu$ m	0.35 $\mu$ m	0.35 $\mu$ m	0.18 $\mu$ m	0.35 $\mu$ m
	Chip Area	7.6 mm <sup>2</sup>	8.9 mm <sup>2</sup>	20.0 mm <sup>2</sup>	11.3 mm <sup>2</sup>	9.0 mm <sup>2</sup>

Figure 28.1.7: Benchmark with other CMOS-based PoU systems.